Circulation: Cardiovascular Imaging

ORIGINAL ARTICLE

Tropoelastin

A Novel Marker for Plaque Progression and Instability

See Editorial by Duivenvoorden and Mulder

Alkystis Phinikaridou, PhD*
Sara Lacerda, PhD*
Begoña Lavin, PhD
Marcelo E. Andia, MD, PhD
Alberto Smith, PhD
Prakash Saha, PhD, FRCS
René M. Botnar, PhD

BACKGROUND: Elastolysis and ineffective elastogenesis favor the accumulation of tropoelastin, rather than cross-linked elastin, in atherosclerotic plaques. We developed gadolinium-labeled tropoelastin-specific magnetic resonance contrast agents for tropoelastin imaging in animal models.

METHODS AND RESULTS: Two peptides, VVGSPSAQDEASPLS and YPDHVQYTHY, were selected to target tropoelastin. In vitro binding, relaxivity, and biodistribution experiments enabled characterization of the probes and selecting the best candidate for in vivo magnetic resonance imaging. Magnetic resonance imaging was performed in atherosclerotic apolipoprotein E–deficient mice and New Zealand white rabbits with stable and rupture-prone plaques using a gadolinium-labeled tropoelastin-specific magnetic resonance contrast agent. In addition, human carotid endarterectomy specimens were imaged ex vivo. The VVGSPSAQDEASPLS-based probe discriminated between tropoelastin and cross-linked elastin (64%±7% versus 1%±2%; P=0.001), had high in vitro relaxivity in solution ($r_{1\text{-free}}$=11.7±0.6 [mmol/L]$^{-1}$ s^{-1}, $r_{1\text{-bound to tropoelastin}}$=44±1 [mmol/L]$^{-1}$ s^{-1}), and favorable pharmacokinetics. In vivo mice vascular enhancement (4 weeks=0.13±0.007 mm^2, 8 weeks=0.22±0.01 mm^2, 12 weeks=0.33±0.01 mm^2; P<0.001) and R_1 relaxation rate (4 weeks=[0.90±0.01]/s, 8 weeks=[1.40±0.03]/s, 12 weeks=[1.87±0.04]/s; P<0.001) increased with atherosclerosis progression after gadolinium-labeled tropoelastin-specific magnetic resonance contrast agent injection. Conversely, statin-treated (0.13±0.01 mm^2; R_1=[1.37±0.03]/s) and control (0.10±0.005 mm^2; R_1=[0.87±0.05]/s) mice showed less enhancement. Rupture-prone rabbit plaques had higher R_1 relaxation rate compared with stale plaques (R_1=[2.26±0.1]/s versus R_1=[1.43±0.02]/s; P=0.001) after administration of the gadolinium-labeled tropoelastin-specific magnetic resonance contrast agent that allowed detection of rupture-prone plaques with high sensitivity (84.4%) and specificity (92.3%). Increased vascular R_1 relaxation rate was observed in carotid endarterectomy plaques after soaking (R_{1pre}=[1.1±0.26]/s versus R_{1post}=[3.0±0.1]/s; P=0.01). Ex vivo analyses confirmed the magnetic resonance imaging findings and showed uptake of the contrast agent to be specific for tropoelastin.

CONCLUSIONS: Magnetic resonance imaging of tropoelastin provides a novel biomarker for atherosclerotic plaque progression and instability.

*Drs Phinikaridou and Lacerda contributed equally to this work.

Key Words: atherosclerosis ■ elastin ■ gadolinium ■ magnetic resonance imaging ■ tropoelastin

https://www.ahajournals.org/journal/circimaging

CLINICAL PERSPECTIVE

A tropoelastin-binding peptide labeled with gadolinium is a novel probe for molecular imaging of dysfunctional elastogenesis by in vivo magnetic resonance imaging. Our new probe combined with quantitative T_1 mapping may be used as a new imaging biomarker to quantify ineffective elastogenesis related to plaque progression and instability and identify plaques that may be susceptible to rupture. Molecular imaging of tropoelastin using our presented imaging approach may provide information on plaque progression and instability and for monitoring the effectiveness of established and novel interventions in different animal models and human tissue. We showed that statins, a widely used intervention, reduced tropoelastin accumulation in atherosclerotic plaques, but the long-term effects on plaque stability remain to be elucidated. Similarly, the effectiveness of novel interventions, that specifically aim elastin remodeling, can be and remain to be investigated using this contrast agent. Importantly, in our work, we implemented magnetic resonance imaging protocols that have already been used in the clinical setting enabling translation of our current findings in bigger animal models of coronary atherosclerosis to identify plaques that may be susceptible to rupture.

Cardiovascular disease accounts for nearly one-third of sudden and premature deaths worldwide.[1] Despite improvements in the management of patients, cardiovascular disease–related deaths are projected to affect 12 million people by 2030.[2] Atherosclerosis is the underlying cause of the majority of cardiovascular events. Atherosclerotic plaque progression involves the dynamic turnover of the extracellular matrix protein, elastin, through elastolysis[3,4] (degradation) and elastogenesis (de novo synthesis).[5–8] Elastolysis[3,4] induced by inflammatory processes that upregulate the expression of elastases[9] has been considered the major pathway for elastin remodeling. Conversely, dysfunctional elastogenesis and its contribution to plaque progression and instability are less understood.[5–8]

Elastin is a highly abundant extracellular matrix protein found in the arterial wall that contributes to 50% of its dry weight.[5] Mature elastin is an insoluble and hydrophobic polymer, with a low turnover rate. Mature elastin is formed by cross-linking of tropoelastin, a 60 to 72 kDa soluble monomer,[10] by lysyl oxidase. Mature elastin contains several tropoelastin molecules. Tropoelastin has 2 alternating domains: (1) hydrophilic, cross-linked, domains rich in Lys and Ala; and (2) hydrophobic domains (responsible for elasticity) rich in Val, Pro, and Gly, which often occur in repeats of VPGVG or VGGVG.[10] Endothelial cells, vascular smooth muscle cells, and adventitial fibroblasts produce tropoelastin during the late fetal and early neonatal periods of life, after which elastogenesis ceases.[10] Secreted tropoelastin is chaperoned to the extracellular space by the elastin-binding protein [11,12] where tropoelastin is stabilized and aligned along microfibrils, that contain glycoproteins (eg, fibrillins) and microfibril-associated glycoproteins (eg, microfibril-associated glycoprotein-1) before enzymatic cross-linking.[13,14] Thus, normal arteries contain cross-linked elastin but negligible amounts of tropoelastin.

Dysfunctional extracellular matrix synthesis and degradation contribute to the initiation, progression, and complication of arterial diseases, including atherosclerosis,[6,15,16] abdominal aortic aneurysm,[17] supravalvular aortic stenosis,[18] in-stent restenosis,[19,20] and Marfan syndrome.[21] In atherosclerosis, vascular smooth muscle cells[22,23] and macrophages[6,8] resume production of tropoelastin that often fails to cross-link into elastic fibers as a result of the reduced expression or absence of lysyl oxidase[24–29] or any of the components of the microfibrillar scaffold required for fiber assembly.[30–32] Simultaneously, elastin degradation by elastases[9] generates elastin-derived peptides, including the VGVAPG, that are chemotactic for inflammatory cells,[33] participate in lipoprotein retention, and upregulate matrix metalloproteinases,[5] all of which are involved in the progression and instability of a plaque.

During the past 10 years, there have been significant developments in imaging of molecular components of the vessel wall in vivo. Imaging of vascular elastin has been achieved using the elastin-specific magnetic resonance imaging (MRI) contrast agent (ESMA)[34] in preclinical models of atherosclerosis,[35–37] abdominal aortic aneurysm,[38] coronary artery injury,[39] and myocardial remodeling after infarction.[40,41] Collagen-binding paramagnetic nanoparticles have also successfully been used to image collagen remodeling in murine atherosclerosis[42]; while in vivo optical analysis has been used to quantify changes in collagen and elastin after wall injury.[43]

As elastogenesis and elastolysis favor the accumulation of tropoelastin, rather than fully processed cross-linked elastin, we hypothesized that tropoelastin may serve as a new imaging biomarker to detect atherosclerosis progression and lesion instability. Herein, we have developed, characterized, and validated novel tropoelastin-specific MR contrast agents to image tropoelastin turnover in models of atherosclerosis and plaque instability and shown potential to bind to symptomatic plaques taken from patients undergoing carotid endarterectomy.

METHODS

The data, analytic methods, and study materials will not be made available to other researchers for purposes of reproducing the results or replicating the procedure.

Elastin and Tropoelastin-Binding Probes

The tropoelastin peptides were selected as described in the Methods in the Data Supplement. The probes, (DOTA)-VVGSPSAQDEASPLS and K(DOTA)YPDHVQYTHY, their corresponding scrambled versions DOTA-GAESAPLVSSVQSPD (scrambled-V) and K(DOTA)-HQVYTYPHDY (scrambled-Y), as well as the rhodamine-labeled VVGSPSAQDEASPLS peptide derivative were custom synthesized by Peptide Synthetics Ltd (Hampshire, United Kingdom). The DOTA peptides were complexed in house with lanthanide ions: europium (Eu^{3+}), lanthanum (La^{3+}), or gadolinium (Gd^{3+}) for in vitro binding assays, relaxivity, and MRI experiments or $^{64}Cu^{2+}$ for biodistribution studies. The complexed (DOTA)-VVGSPSAQDEASPLS and K(DOTA)YPDHVQYTHY probes were denominated as tropoelastin-binding MR contrast agents (TESMAs). The diethylenetriaminepentaacetic acid (DTPA)–based elastin-specific contrast agent was provided by Lantheus Medical Imaging (North Billerica),[34] either complexed to gadolinium (Gd-ESMA; 856 Da) for relaxivity and MRI experiments or in its free form (ESMA), complexed in house with Eu^{3+} for in vitro binding assays. Eu^{3+}-labeled DTPA solutions (Eu-DTPA) complexed in house were used as controls.

Synthesis of the lanthanide(III) complexes, in vitro binding, and relaxivity studies were performed as described in the Methods in the Data Supplement.

Murine Model of Atherosclerosis Progression

Male apolipoprotein E knockout ($ApoE^{-/-}$) mice and wild-type (WT) C57BL/6J were purchased from Charles Rivers Laboratories (Edinburgh, United Kingdom). Eight-week-old $ApoE^{-/-}$ mice were switched to a high-fat diet (HFD) containing 21% fat from lard and 0.15% (wt/wt) cholesterol (Special Diets Services, Witham, United Kingdom). $ApoE^{-/-}$ mice were imaged at 4, 8, and 12 weeks after HFD feeding (n=10 per group). In the treatment group, $ApoE^{-/-}$ mice (n=10) received pravastatin (40 mg/kg per day; Kemprotec Ltd, Middlesborough, United Kingdom) administered in the drinking water simultaneously with the HFD for 12 weeks. Eight-week-old WT mice (n=10) were fed a normal chow diet for 12 weeks and scanned at 20 weeks.

Rabbit Model of Plaque Instability

Six 3-month-old male New Zealand White rabbits (Harlan, Wyton, England; mean weight, 2.5 kg) were fed a 1% cholesterol diet (Special Diet Services, Witham, England) for 2 weeks before and 6 weeks after balloon injury of the abdominal aorta. This was followed by 4 weeks of normal chow diet as previously described.[36,44,45] Diseased rabbits received intraperitoneal administration of Russell's viper venom (0.15 mg/kg; Enzyme Research Laboratories, Swansea, United Kingdom), a procoagulant factor, followed 30 minutes later by intravenous administration of histamine dihydrochloride (0.02 mg/kg; Sigma-Aldrich, Dorset, England), a vasoconstrictor in rabbits, to induce plaque disruption and thrombosis. This procedure was repeated twice within 4 hours. All procedures were approved by the United Kingdom Home Office and were in accordance with institutional guidelines.

Biodistribution of ^{64}Cu-Labeled Tropoelastin Probes

Biodistribution experiments are described in the Methods in the Data Supplement.

In Vivo Molecular Imaging of Tropoelastin at 3T

All imaging experiments were performed using a 3T Philips Achieva MR scanner (Philips Healthcare, Best, The Netherlands) equipped with a clinical gradient system (30 mT/m, 200 mT/m per millisecond).

Mice

Mice (n=10 per group) were imaged using a single-loop surface coil (diameter=23 mm). The animals were placed in prone position, and the brachiocephalic artery was imaged 30 to 40 minutes post-injection of the tropoelastin-binding contrast agent Gd-TESMA ([Gd-DOTA]-VVGS; 0.2 mmol/kg). A subgroup of animals (n=5 per group) was also scanned 1 hour (optimal time point) after injection of Gd-ESMA (0.2 mmol/kg) on the previous day for comparison (Figure IA in the Data Supplement). In addition, 12 weeks HFD-fed animals (n=3) were imaged 30 to 40 minutes after injection of the scrambled-VVGS probe (0.2 mmol/kg), and another 2 mice were imaged with a 1:1 (Gd-TESMA+La-TESMA) cocktail for in vivo competition experiments. A detailed MRI acquisition protocol is described in the Methods in the Data Supplement.

Rabbits

The abdominal aorta of diseased rabbits was scanned using a 32-channel cardiac coil. Rabbits received general anesthesia and were imaged in a supine position twice before (pre) and 1 time after (post) pharmacological triggering (Figure IB in the Data Supplement). The pretrigger MRI included 2 separate scanning sessions: 1 before and after administration of Gd-ESMA and 1 before and after administration of Gd-TESMA. The second MRI session was performed 2 days after the first to allow vessel wall clearance of Gd-ESMA. During these sessions, native zoom T1-weighted black-blood (BB) and delayed-enhanced (DE) images and T1 maps were acquired 2 hours after administration of Gd-ESMA (0.2 mmol/kg) and 40 minutes after administration of Gd-TESMA (0.2 mmol/kg). After the second scan, the rabbits were triggered twice for plaque rupture and the final post-triggering MRI session was performed 8 hours later. The post-trigger MRI included acquisition of native zoom T1-weighted BB images to visualize thrombus. A detailed MRI acquisition protocol is described in the Methods in the Data Supplement.

Ex Vivo T1 Mapping Experiments Using Symptomatic Plaques Taken From Patients Undergoing Carotid Endarterectomy at 3T

Fresh symptomatic carotid endarterectomy specimens were imaged before and after soaking them in Gd-TESMA (Figure IC in the Data Supplement). A detailed tissue handling and MRI acquisition protocol are described in the Methods in the Data Supplement. Collection and use of human samples were approved by an institutional review committee, and subjects gave informed consent.

MRI Analysis

In mice, vessel wall area was calculated by manually segmenting the visually enhanced region of the vessel wall as seen on the DE-MRI images using OsiriX (OsiriX Foundation, Geneva, Switzerland). To ensure that the segmented area encompassed the vessel wall, the DE-MRI were coregistered and fused with the magnetic resonance angiography images. T_1 values were computed on a pixel-by-pixel basis using a 3-parameter fit implemented in Matlab.[35] In rabbits, pretrigger native T1-weighted (T1w)-BB images and contrast enhanced inversion recovery and T1 maps were used to assess the vascular remodeling. Post-trigger native T1w-BB images were only used to identify the presence or absence of thrombus as an end point for the classification of plaques as rupture-prone and stable, respectively. The T1 maps were automatically generated after the data acquisition using a 3-parameter fit model. The T1 maps were imported into Osirix, and the vessel wall was manually segmented to calculate the R_1. When segmenting the T1 maps, the anatomic T1w-BB images were used to aid the identification of the vessel wall contours. The analysis was performed on anonymized data sets in all experiments. T1 maps of ex vivo carotid endarterectomy specimens were analyzed as described above for the rabbit images.

Histology

Mice

The aortic root, aortic arch, brachiocephalic, and carotid arteries were removed en bloc, pinned down to maintain tissue morphology, and fixed in 10% formaldehyde for 48 hours (n=4 per group). Tissues were embedded in paraffin and sectioned transversely (5-µm thick). Verhoeff-Van Gieson elastin staining (HT25A-1KT, Sigma, Dorset, United Kingdom) and Trichrome Stain (Masson) Kit (HT15-1KT, Sigma, Dorset, United Kingdom) were used to investigate vessel wall morphology and elastin and collagen fibers, respectively. Immunohistochemistry for tropoelastin was performed using an anti-mouse rabbit polyclonal antibody (1:100, Abcam, ab21600, Cambridge, MA). Vessel wall area was calculated using the Verhoeff-Van Gieson images as (adventitia area–the luminal area [mm^2]) using ImageJ (National Institutes of Health). The immunopositive areas were segmented and expressed as normalized tropoelastin area (%tropoelastin=tropoelastin immunopositive area/vessel wall area)×100. Fluorescent microscopy was performed using a custom-synthesized rhodamine-labeled VVGS peptide derivative (rhod-VVGS). Sections were incubated with a 200 nmol/L solution for 24 hours at 4°C followed by nuclear counterstain using Hoechst (ThermoFischer 33342, 1:3000, for 15 minutes at room temperature). Slides were shielded from light at all times and mounted with a Mowiol containing 2.5% 1,4-diazobicyclo-[2.2.2]-octane (DABCO, Sigma, D2522) medium.

Rabbits

Transverse cryosections (10-µm thick) were collected throughout the length of each segment at 500 µm intervals and stained with Verhoeff-Van Gieson to visualize the elastin fibres and calculate the total elastin content. Immunohistochemistry for tropoelastin was performed using an anti-mouse rabbit monoclonal antibody (1:100, NB100-2076, Novus Biologicals, Abingdon, United Kingdom). Computer-assisted color image analysis (ImageJ) was used to quantify the percentage total elastin and tropoelastin content, using the Verhoeff-Van Gieson elastin and tropoelastin immunohistochemistry stainings, respectively. For registration of the in vivo MRI and histological sections, the distance of the proximal end of each segment from the renal branches and iliac bifurcation, the gross morphology, and internal plaque or thrombus landmarks visible on both the MR and histological images were used as references.

Human Carotid Endarterectomy Specimens

After the imaging experiments, the plaques from endarterectomy were fixed in formalin, decalcified, embedded in paraffin, and sectioned transversely at 5µm. Sections were stained for collagen using Masson trichrome, elastin with Verhoeff-Van Gieson, and tropoelastin by immunohistochemistry (1:100, Abcam, ab21600, Cambridge, MA).

Western Blot experiments for quantification of vessel wall tropoelastin concentration are described in the Methods in the Data Supplement.

Inductively coupled plasma mass spectrometry was used to quantify vessel wall gadolinium concentrations as described in the Methods in the Data Supplement.

Statistical Analyses

The detailed statistical methods are described in the Methods in the Data Supplement. $P<0.05$ was considered statistically significant.

RESULTS

Chemical Structures and In Vitro Binding Assays

The chemical structures and molecular weight of the gadolinium-labeled tropoelastin-binding probes are shown in Figure 1A and 1B.

In vitro binding experiments showed that both K(Eu-DOTA)-YPDH and (Eu-DOTA)-VVGS probes have high selectivity toward tropoelastin compared with other proteins, including collagen I, fibronectin, and HSA (human serum albumin; Figure 1C). Importantly, the (Eu-DOTA)-VVGS probe showed superior discrimination

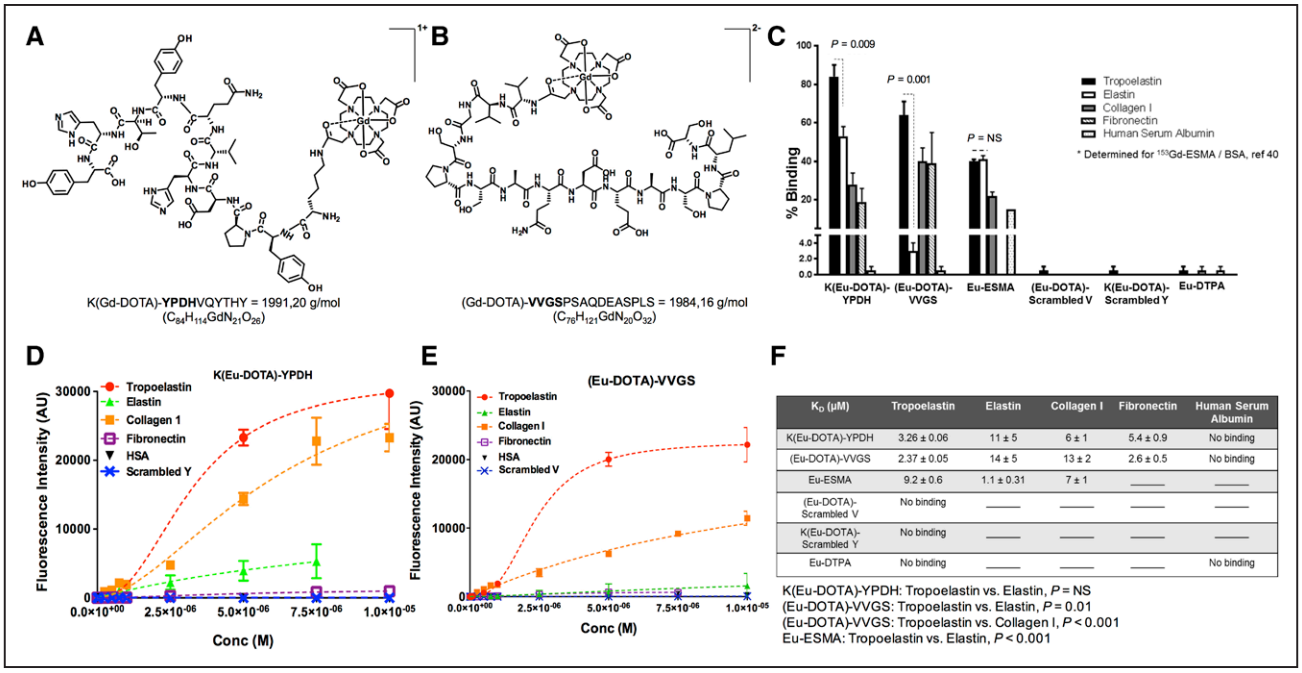

K_D (μM)	Tropoelastin	Elastin	Collagen I	Fibronectin	Human Serum Albumin
K(Eu-DOTA)-YPDH	3.26 ± 0.06	11 ± 5	6 ± 1	5.4 ± 0.9	No binding
(Eu-DOTA)-VVGS	2.37 ± 0.05	14 ± 5	13 ± 2	2.6 ± 0.5	No binding
Eu-ESMA	9.2 ± 0.6	1.1 ± 0.31	7 ± 1	____	____
(Eu-DOTA)-Scrambled V	No binding	____	____	____	____
K(Eu-DOTA)-Scrambled Y	No binding	____	____	____	____
Eu-DTPA	No binding	____	____	____	No binding

Figure 1. Chemical structures and in vitro binding experiments of the tropoelastin-binding probes. **A** and **B**, Chemical structures of the probes. **C**, In vitro binding show superior discrimination between tropoelastin and mature elastin for the (Eu-DOTA)-VVGS compared with K(Eu-DOTA)-YPDH whereas Eu-elastin-specific magnetic resonance contrast agent (ESMA) binds equally to tropoelastin and mature elastin. The new probes show less binding toward other proteins compared with tropoelastin whereas the scrambled peptides do not bind to tropoelastin. Eu-DTPA shows little binding to tropoelastin, collagen I, and human serum albumin. **D**–**E**, The saturation binding plots show that both probes bind to tropoelastin whereas no binding to human serum albumin (HSA) was observed. Finally, no binding of the scrambled probes to tropoelastin was observed. **F**, The K_D values showed that the probes have high affinity for tropoelastin. Statistical differences between Kd values are shown. No binding signifies that the data could not be fit, and lines indicate that the assay was not performed (n=2 for elastin, n=3 for all other proteins). AU indicates arbitrary units; Eu, europium(III).

between tropoelastin and mature elastin (64%±7% versus 1%±2%; *P*=0.001) compared with K(Eu-DOTA)-YPDH (84%±4% versus 53%±5%; *P*=0.009). Conversely, Eu-ESMA showed equal binding to tropoelastin and mature elastin (40%±1% versus 41%±2%; *P*=NS). In addition, both (Eu-DOTA)-VVGS and K(Eu-DOTA)-YPDH did not show binding to HSA, whereas Eu-ESMA has been reported to bind 15% to HSA (value included in Figure 1C[39]). Finally, Eu-DTPA and complexes of the scrambled VVGS and YPDH probes showed no binding to all proteins studied. The saturation binding plots (Figure 1D and 1E) showed that both probes bind to tropoelastin whereas no binding to HSA was observed. Finally, no binding of the scrambled probes to tropoelastin was observed. The K_D values showed high affinity of the probes toward tropoelastin (Figure 1F). Further competition studies showed the specificity of the 2 probes (Figure II in the Data Supplement).

Relaxivity Studies Using Gd-Labeled Tropoelastin and Elastin-Binding Contrast Agents

^{1}H nuclear magnetic relaxation dispersion profiles obtained in PBS were characteristic of small-molecular weight complexes (Figure 2A–2C). As expected, the relaxivity values of the new probes were higher (r_1=8.9±0.4 and 11.7±0.6 [mmol/L]$^{-1}$·s^{-1} for K(Gd-DOTA)-YPDH and (Gd-DOTA)-VVGS, respectively, at 20 MHz and 37°C) compared with nonpeptide based contrast agents (eg, Gd-DTPA=4.02 [mmol/L]$^{-1}$·s^{-1} at 20 MHz, 37°C)[46] (Figure 2D) because of the increased molecular weight (reducing the rotational correlation time), which also contributes to second- and outer-sphere proton relaxation effects.[46] The relaxivity of Gd-ESMA was measured to be 4.9±0.3 (mmol/L)$^{-1}$·s^{-1} (20 MHz, 37°C).

In the presence of tropoelastin, the relaxivity of the bound fraction was calculated taking into account the K_D and a stoichiometry of 1:2 tropoelastin:probe as determined by the fluorescence studies (Figure 1F) and was plotted as a function of the magnetic field strength (Figure 2A–2C). These nuclear magnetic relaxation dispersion profiles correspond to slow tumbling systems with a typical high field peak ≈20 to 40 MHz showing overall higher relaxivity for the tropoelastin-bound fraction: 36±1, 44±1, and 25±1 (mmol/L)$^{-1}$·s^{-1} for tropoelastin-[K(Gd-DOTA)-YPDH)], tropoelastin-[(Gd-DOTA)-VVGS)], and tropoelastin-[(Gd-ESMA)], respectively.

To investigate the metabolic stability of all Gd-probes, we measured the R_1 relaxation rates of 1 mmol/L solution of the probes incubated with murine and human blood and plasma every 30 minutes, up to

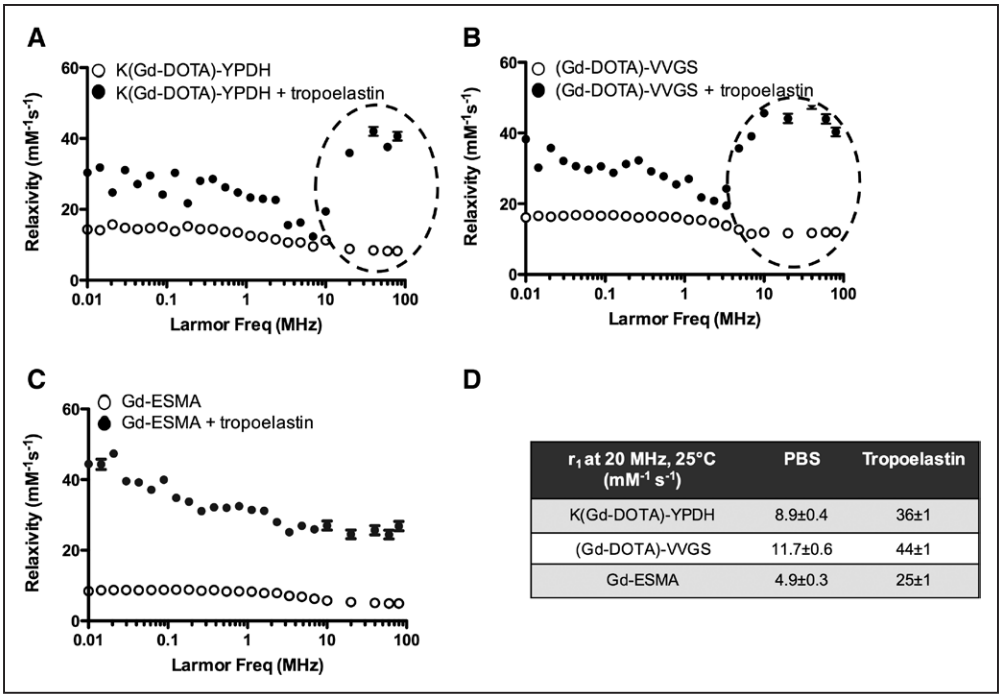

r_1 at 20 MHz, 25°C (mM^{-1} s^{-1})	PBS	Tropoelastin
K(Gd-DOTA)-YPDH	8.9±0.4	36±1
(Gd-DOTA)-VVGS	11.7±0.6	44±1
Gd-ESMA	4.9±0.3	25±1

Figure 2. Relaxivity studies and nuclear magnetic relaxation dispersion (NMRD) profiles of Gd-labeled tropoelastin and elastin-binding contrast agents at 20 MHz and 37°C. **A**–**C**, ^{1}H-NMRD in the absence (○) and presence (●) of tropoelastin. The profiles obtained in PBS (○) are characteristic of small-molecular weight complexes. In the presence of tropoelastin (●), the relaxivity increases, suggesting binding of the probes to the protein. The relaxivity increase was more evident for both (Gd-DOTA)-VVGS and K(Gd-DOTA)-YPDH compared with Gd-elastin-specific magnetic resonance contrast agent (ESMA). **D**, Summary of the relaxivity values (n=3 for all studies).

4 hours at 3T. These data showed that the probes were stable in solution for up to 4 hours as the changes in the R_1 relaxation rate were not statistically significant (data not shown).

Biodistribution of ^{64}Cu-Labeled Tropoelastin Probes

Biodistribution studies showed favorable pharmacokinetics with high renal clearance for both probes and some liver uptake for the K(^{64}Cu-DOTA)-YPDH (Figure III in the Data Supplement).

In Vivo Comparison of Vessel Wall Enhancement by MRI Using the Elastin (ESMA) and Tropoelastin Binding (TESMA) Contrast Agent

Considering that (Gd-DOTA)-VVGS was superior in differentiating tropoelastin from cross-linked elastin and had less liver uptake compared with the K(DOTA)-YPDH imaging probe, the (Gd-DOTA)-VVGS, denominated as Gd-TESMA, was selected as the best candidate for in vivo molecular imaging of tropoelastin by MRI. For initial in vivo MRI experiments, control and atherosclerotic ApoE$^{-/-}$ mice were scanned, after the administration of Gd-ESMA, and 24 hours later, after the administration of Gd-TESMA (Figure 3). Pilot studies showed clearance of Gd-ESMA from both the blood and vessel wall after 24 hours (data not shown). Fused maximum intensity projection magnetic resonance angiography and DE images after injection of Gd-TESMA showed focal uptake in the brachiocephalic artery of an atherosclerotic mouse (Figure 3A). DE-MRI of the brachiocephalic artery acquired from a control animal after injection of Gd-ESMA showed vessel wall enhancement (Figure 3B and 3C) as Gd-ESMA binds to endogenously found cross-linked elastin, present in nondiseased arteries. Conversely, there was no enhancement of the control vessel wall after injection of Gd-TESMA because of the lack of tropoelastin in the absence of disease (Figure 3D and 3E). However, 2 different atherosclerotic mice showed enhancement of the vessel wall after administration of both Gd-ESMA and Gd-TESMA (Figure 3F–3M). DE-MRI showed a larger area of enhancement after administration of Gd-ESMA compared with Gd-TESMA as the diseased vessel wall contains a mixture of cross-linked elastin and tropoelastin and Gd-ESMA binds to both fractions whereas Gd-TESMA only binds to tropoelastin (also see Figure 1C; Figure IVA and IVB in the Data Supplement).

In vivo molecular MRI of tropoelastin shows accumulation of tropoelastin during atherosclerosis progression in mice. DE-MRI (Figure 4A$_1$–4D$_1$ and 4A$_2$–4D$_2$) and R_1 maps (Figure 4A$_3$–4D$_3$) acquired after administration of Gd-TESMA showed progressive enhancement and increased vessel wall R_1 relaxation rate of the brachiocephalic artery in ApoE$^{-/-}$ mice exposed to an HFD

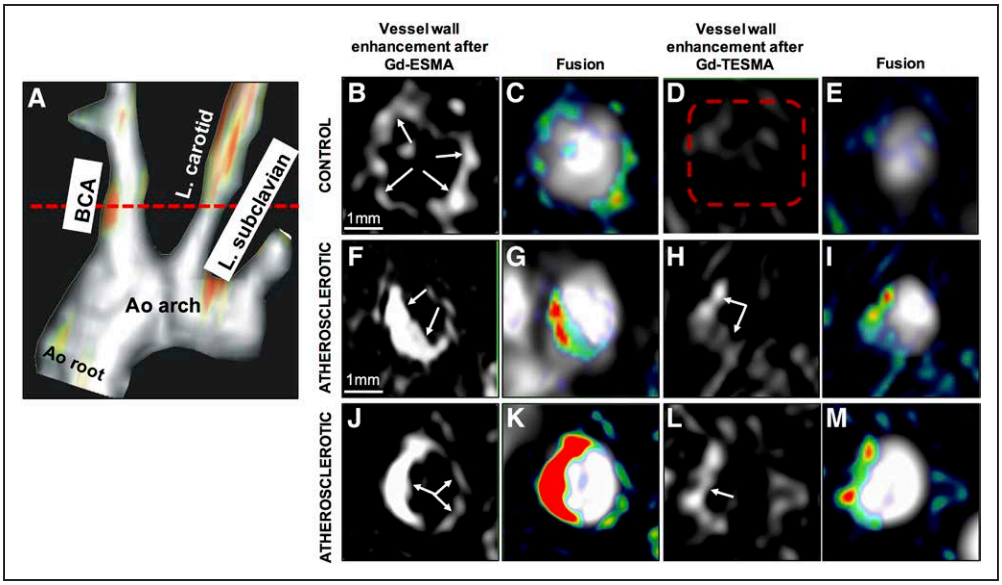

Figure 3. In vivo magnetic resonance imaging (MRI) comparison of vessel wall enhancement using the elastin (elastin-specific magnetic resonance contrast agent [ESMA]) and tropoelastin (TESMA) binding contrast agents in mice. **A**, Fused maximum intensity projection (MIP) reconstructed magnetic resonance angiography and delayed-enhanced-MRI after administration of Gd-TESMA show focal uptake of Gd-TESMA in the brachiocephalic artery (BCA) of an atherosclerotic apolipoprotein E–deficient mouse. **B**–**E**, MRI of the BCA acquired from a control animal, scanned 24 h apart, showed vessel wall uptake of Gd-ESMA (**B** and **C**), but no uptake of Gd-TESMA (**D** and **E**) because of the lack of tropoelastin in the absence of disease. **F**–**M**, MRI of the BCA acquired from 2 different diseased animals showed enhancement of the vessel wall after administration of both agents because of the presence of both cross-linked elastin and tropoelastin in the atherosclerotic lesion. Ao indicates aortic; and L., left (n=5 per group).

compared with WT mice. Statin-treated ApoE$^{-/-}$ mice showed significantly less enhancement and lower relaxation rate compared with untreated ApoE$^{-/-}$ mice (Figure 4E$_1$–4E$_3$). The uptake of Gd-TESMA by DE-MRI and R$_1$ mapping paralleled the growth of atherosclerotic lesions (Figure 4A$_4$–4E$_4$) as seen by Van Gieson elastin staining and the deposition of tropoelastin fibers as seen by immunostaining (Figure 4A$_5$–4E$_5$, 4A$_6$–4E$_6$,and 4A$_7$–4E$_7$). The higher magnification images (Figure 4A$_6$–4E$_6$) of tropoelastin immunopositive areas (black signal) show that the antibody does not bind to endogenously and cross-linked elastin found in the media of control arteries and even in tissues from animals fed with an HFD for 4 weeks. However, as the disease progresses and new tropoelastin fibers are deposited within the growing intima, and also as media elastin becomes fragmented by elastases, the immunopositive areas increase in both of these layers of the vessel wall. ApoE$^{-/-}$ mice fed an HFD for 12 weeks showed less vessel wall enhancement after administration of the scrambled peptide probe (DOTA-GAESAPLVSSVQSPD) compared with those injected with the nonscrambled probe (Figure 4F$_1$–4F$_3$). In vivo competition experiments showed displacement of the (Gd-DOTA)-VVGS probe by the (La-DOTA)-VVGS probe in the brachiocephalic artery of atherosclerotic mice (Figure V in the Data Supplement). Ex vivo fluorescent microscopy experiments showed fluorescent signal originating from the rhodamine-labeled VVGS peptide derivative within tropoelastin-rich areas of diseased vessels as identified by corresponding immunohistochemistry. Conversely, fluorescent signal originating from the probe was found to be nearly nonexistent in the regions containing mature/crosslink elastin-rich and collagen in diseased vessels (Figure VI the Data Supplement).

Quantitative MRI, Histology, and Western Blot Measurements of Murine Vessel Wall Tropoelastin

Quantification of the MR data showed that the DE-MRI area(Figure5A;control=0.10±0.005,4weeks=0.13±0.01, 8weeks=0.22±0.01,12weeks=0.33±0.01mm^2;*P*<0.001) and the vessel wall R$_1$ (Figure 5B; control=0.87±0.05, 4 weeks=0.90±0.01, 8 weeks=1.40±0.03, 12 weeks=1 .87±0.04/s; *P*<0.001) significantly increased with disease progression and decreased with statin treatment (DE-MRI treated=0.13±0.01 mm^2, R$_1$ treated=[1.37±0.03]/s). Less uptake was found in 12-week-old HFD-fed ApoE$^{-/-}$mice injected with a scrambled peptide of VVGS (0.13±0.01 versus 0.33±0.01 mm^2; *P*=0.001) and lower R$_1$ (0.91±0.06 versus 1.87±0.04; *P*=0.01) compared with animals injected with the nonscrambled Gd-TESMA peptide. Segmentation of the tropoelastin immunopositive areas showed a significant accumulation of tropoelastin fibers during atherosclerosis progression and reduction of tropoelastin in the statin-treated ApoE$^{-/-}$ mice (% tropoelastin, control mice=3.8±0.50, 4 weeks HFD=3.74±0.60, 8 weeks HFD=12.10±0.52, 12 weeks HFD=18.54±0.30, statin-treated at 12 weeks with HFD=11.41±0.35; *P*=0.002; Figure 5C). Quantification of the vessel wall gadolinium concentration by

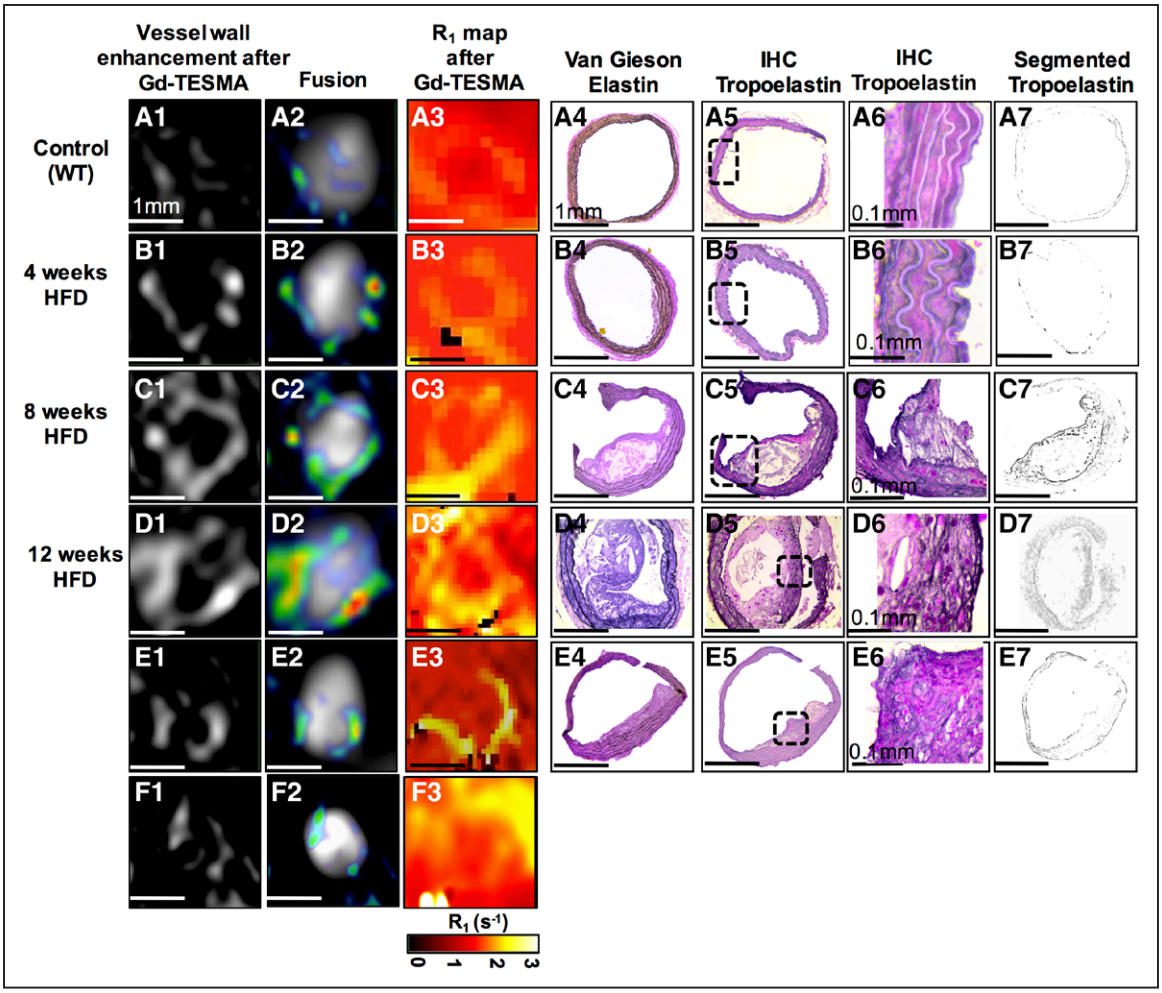

Figure 4. Molecular in vivo magnetic resonance imaging (MRI) of tropoelastin in atherosclerotic mice. **A_1–E_1**, **A_2–E_2**, **A_3–E_3**, Delayed-enhanced (DE)-MRI and R_1 relaxation rate maps after injection of Gd-tropoelastin-specific magnetic resonance contrast agent (TESMA) show progressive enhancement of the brachiocephalic artery and vessel wall relaxation rate with disease progression compared with control and statin-treated mice. **F_1–F_3**, DE-MRI and R_1 maps after injecting the scrambled peptide (DOTA-GAESAPLVSSVQSPD) show less vessel wall enhancement and relaxation rate. **A_4–E_4**, Van Gieson elastin staining shows the development of atherosclerotic lesions. **A_5–E_5**, **A_6–E_6**, and **A_7–E_7**, Immunohistochemistry shows accumulation of tropoelastin molecules (dark purple staining) in the lesion (n=10 per group). HFD indicates high-fat diet; IHC, immunohistochemistry.

inductively coupled plasma mass spectrometry showed similar trends (control=176±50, 4 weeks=165±38, 8 weeks=244±52, 12 weeks=303±38, statin-treated at 12 weeks=207±23 nmol/g tissue; *P*=0.007; Figure 5D). There was a significant correlation between the vessel wall R_1 and gadolinium concentration (*r*=0.97; *P*=0.004; 95% CI, 0.69–0.99). A linear regression analysis of average R_1 and average [Gd] per time point of disease progression revealed an in vivo bound relaxivity of r_1=7.15 $(mmol/L)^{-1}$ s^{-1} (Figure 5E).

We found a significant correlation between the DE-MRI plaque area and vessel wall R_1 measured after administration of Gd-TESMA (*r*=0.58; *P*<0.001; 95% CI, 0.46–0.69; Figure 5F). There were also strong positive correlations between plaque % tropoelastin (measure immunohistochemically) and both the in vivo DE-MRI area (r=0.76; P<0.001; 95% CI, 0.47–0.89; Figure 5G) and vessel wall R_1 (*r*=0.93; *P*<0.001; 95% CI, 0.76–0.96; Figure 5H), suggesting that the increased MRI signal observed in this model reflects the histological accumulation of tropoelastin fibers within the growing lesion.

In addition to the quantification of tropoelastin by immunohistochemistry (Figure 5C), the modulation of the protein levels during atherosclerosis progression and in response to treatment was also measured by Western blotting. Dilutions of recombinant tropoelastin were used to generate a standard curve for the quantification of the tropoelastin concentration from tissue lysates (Figure 5I). Western blotting of purified cross-linked elastin and soluble tropoelastin showed that the cross-linked polymer gives a high molecular weight band (>250 kDa) whereas the tropoelastin monomer has a molecular weight of 70 kDa (Figure 5J). Western blotting of tropoelastin extracted from the vessel wall showed negligible amounts in control arteries and increased deposition during atherosclerosis progression in $ApoE^{-/-}$ mice. Tropoelastin content was decreased in statin-treated $ApoE^{-/-}$ mice (Figure 5J). Quantification of tropoelastin

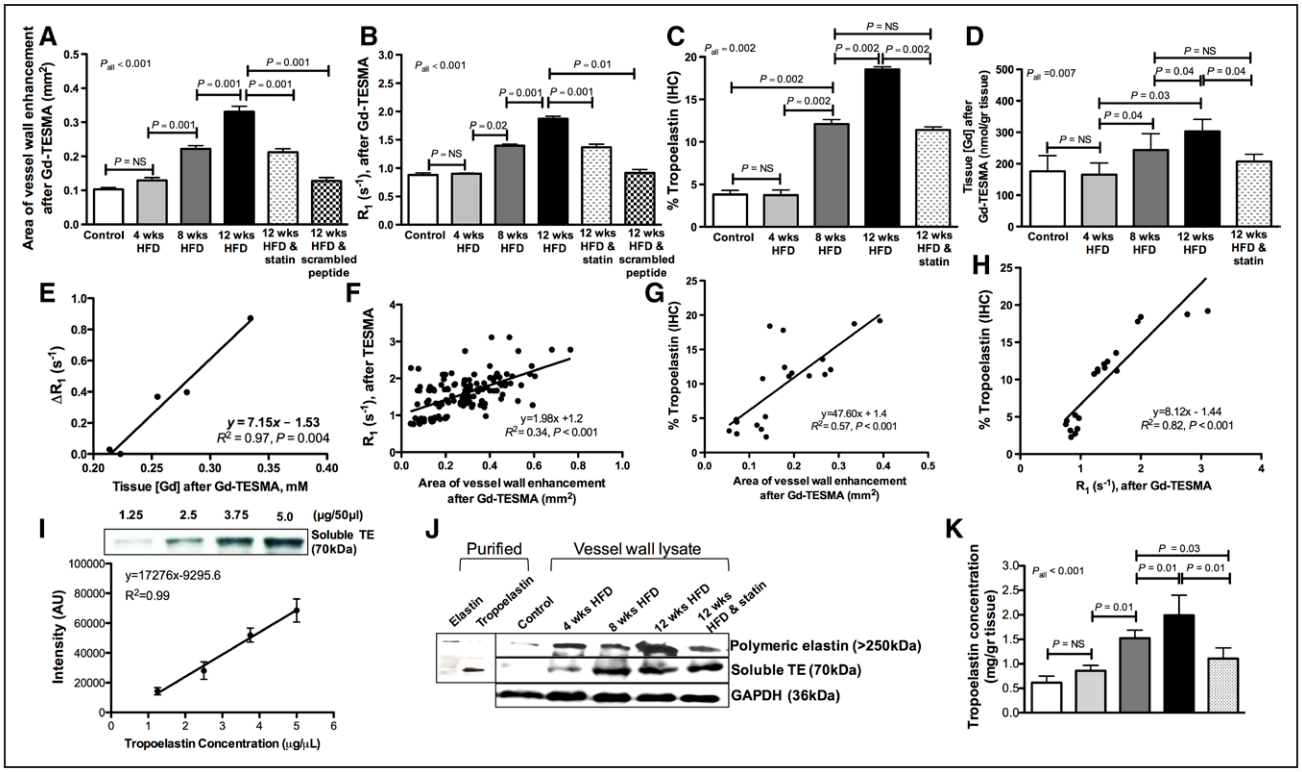

Figure 5. Quantitative magnetic resonance imaging (MRI), histology, and Western blotting of murine vessel wall tropoelastin. **A**–**B**, Delayed-enhanced (DE)-magnetic resonance imaging (MRI) area and vessel wall R_1 measured after administration of Gd-tropoelastin-specific magnetic resonance contrast agent (TESMA) increase with disease progression and decrease with statin treatment (n=10 per group). **C**, Tropoelastin accumulates during atherosclerosis progression and reduces in statin-treated mice (n=4 per group). **D**, Vessel wall gadolinium concentration increases with disease progression (n=4 per group). **E**, The measured in vivo bound relaxivity of TESMA is r_1=7.15 $(mmol/L)^{-1}$ s^{-1}. **F**, DE-MRI area correlates with vessel wall R_1 measured after administration of Gd-TESMA (n=10 per group). The tropoelastin content measured histologically correlates with both the DE-MRI (**G**) and vessel wall R_1 relaxation rate (**H**) measured by MRI after administration of Gd-TESMA (n=4 per group). **I**, Dilutions of recombinant human tropoelastin were used to generate a standard curve for the quantification of the tropoelastin concentration from tissue lysates using Western blotting. **J**, Western blotting of purified elastin showed that cross-linked elastin is an insoluble polymer with a high molecular band (>250 kDa) whereas soluble tropoelastin has a molecular weight at 70 kDa. Western blotting for tropoelastin extracted from the vessel wall (n=3 per group) showed negligible amounts in control arteries and increased deposition of the protein during atherosclerosis progression in apolipoprotein E–deficient ($ApoE^{-/-}$) mice. Tropoelastin content was decreased in the statin-treated $ApoE^{-/-}$ mice. **K**, Quantification of tropoelastin concentration in control and diseased arteries as measured by Western blotting.

concentration in control and diseased arteries is shown in Figure 5K (control=0.62±0.04, 4 weeks=0.86±0.05, 8 weeks=1.52±0.06, 12 weeks=1.99±0.15, statin-treated at 12 weeks=1.17±0.09 mg/g tissue; P<0.001).

In Vivo Molecular MRI of Tropoelastin Allows Detection of Rupture-Prone Rabbit Plaque

To test the ability of molecular MRI of tropoelastin in discriminating between stable and rupture-prone plaques, we used a rabbit model of atherosclerosis and controlled plaque rupture.

Atherosclerosis was observed at 12 weeks in all 6 injured and cholesterol-fed rabbits, and thrombosis occurred in 5 (83%) animals at rates similar to those previously reported.[36,44,45,47] Figure 6 shows corresponding native T1w-BB, DE images, and T_1 maps after administration of Gd-ESMA and Gd-TESMA acquired at 12 weeks and before triggering for plaque rupture and native T1w-BB images acquired after triggering for plaque rupture. Representative pretrigger T1w-BB images of a stable (Figure 6A–6E) and rupture-prone plaques (Figure 6G–6K) show the anatomy of the vessel wall and the location of the plaque. The DE images show an enhancement of the vessel wall and shortening of the T1 relaxation time both after the administration of Gd-ESMA and also after the administration of Gd-TESMA. The corresponding T1w-BB images acquired after triggering show the lack of thrombus at the level of the stable plaque and the presence of thrombus at the location of the rupture-prone lesion (Figure 6F and 6L). Although both Gd-ESMA and Gd-TESMA lead to vessel wall enhancement, quantitative assessment of the R_1 relaxation rate showed that the uptake of contrast agent was significantly different between stable and rupture-prone lesions only after administration of Gd-TESMA (Figure 6M). Rupture-prone plaques uptake significantly more Gd-TESMA compared with stable plaques (R_1=2.26±0.1 versus R_1=1.43±0.02; P=0.001) whereas the uptake of Gd-ESMA was similar between stable and rupture-prone plaques (R_1=2.14±0.05 versus R_1=2.44±0.07; P=NS).

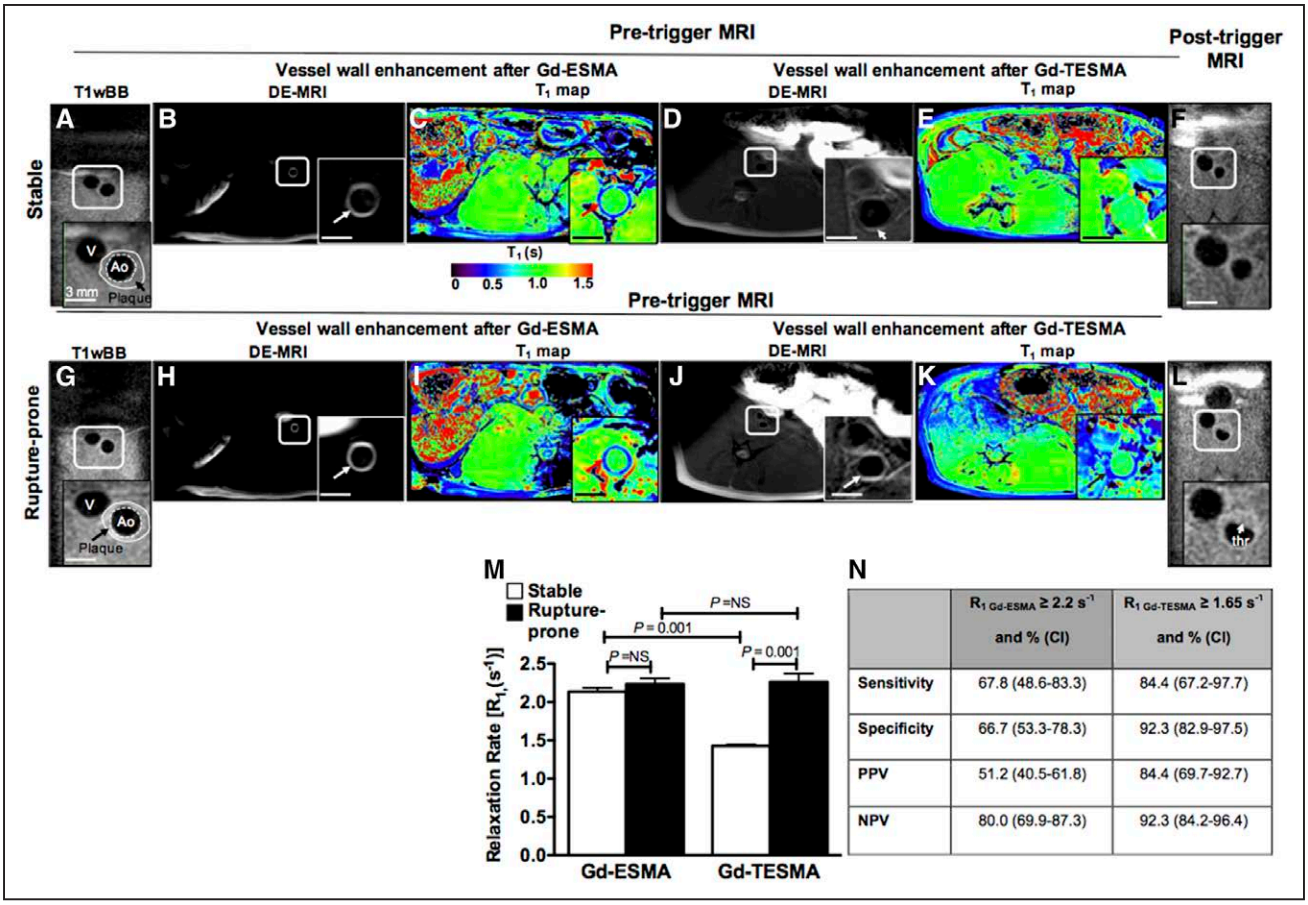

Figure 6. In vivo molecular magnetic resonance imaging (MRI) of tropoelastin allows detection of rupture-prone rabbit plaque. Pre-trigger and post-trigger MRI of rabbit stable (**A**–**F**) and rupture-prone (**G**–**L**) plaques. **A** and **G**, Pre-trigger native zoom T1-weighted black-blood (BB) images show the plaque. **B**, **H**, **C**, and **I**, Delayed-enhanced (DE) inversion recovery images and T_1 maps after administration of Gd-elastin-specific magnetic resonance contrast agent (ESMA) show a strong enhancement of the aortic wall and shortening of the T_1 relaxation time in both stable and rupture-prone plaque. **D**, **J**, **E**, and **K**, Corresponding delayed-enhanced inversion recovery images after administration of Gd-tropoelastin-specific magnetic resonance contrast agent (TESMA) show vessel wall enhancement and lower T1 values in ruptured-prone compared with stable plaque. **F** and **L**, Corresponding native zoom T1-weighted-BB, post-trigger images show the presence of thrombus only at the side of the ruptured plaque. **M**, Quantification of vessel wall R_1 relaxation rate show a significantly higher R_1 value in rupture-prone compared with stable plaque only after administration of Gd-TESMA. NPV indicates negative predictive value; PPV, positive predictive value.

The sensitivity, specificity, positive predictive value, and negative predictive value of the quantitative assessment of vascular elastin and tropoelastin (R_1) after administration of Gd-ESMA and Gd-TESMA, respectively, in detecting the rupture-prone plaque are tabulated in Figure 6N. These measurements suggest that quantitative assessment of vessel wall contrast uptake using T_1 mapping after administration of Gd-TESMA allows better in vivo detection of rupture-prone plaques.

Histological Analyses Show Accumulation of Tropoelastin in Rabbit Rupture-Prone Compared With Stable Plaque

Histological analyses of rabbit sections using Van Gieson elastin showed multiple elastin lamellae consisting of mature, cross-linked elastin in control arteries (Figure 7A; black stain), but no corresponding immunopositive tropoelastin fibers suggesting the antibody is specific for monomeric tropoelastin (Figure 7B and 7C).

In both stable and ruptured plaques, there was deposition of elastin in the intima (Figure 7D and 7G), and in ruptured plaques, there was also additional disintegration and fragmentation of the media elastin as seen by Van Gieson elastin. Immunohistochemistry for tropoelastin (brown stain) showed deposition of tropoelastin in the intima of stable plaque (Figure 7E and 7F) and a more extensive network of tropoelastin in the intima of ruptured plaque (Figure 7H and 7I). In addition, there were immunopositive tropoelastin areas in the media of ruptured plaques that could be because of either deposition of new tropoelastin fibers or exposure of the tropoelastin epitope when mature elastin fibers become fragmented by elastases. Quantification of total elastin and tropoelastin (Figure 7J and 7K) showed that measuring the tropoelastin accumulation in the vessel wall allowed a better discrimination between stable and ruptured plaques (16.6±3.14 versus 42.2±4.0; P=0.001) compared with measuring the net increase of elastin (28.8%±3.0% versus

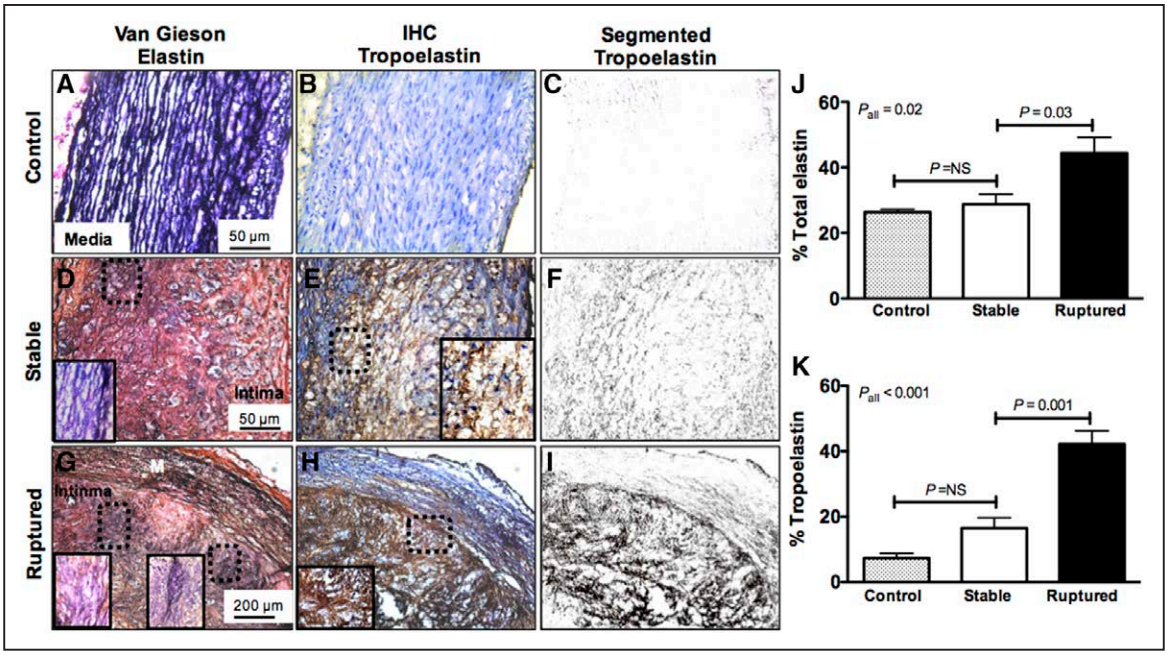

Figure 7. Histological analyses show accumulation of tropoelastin in rabbit rupture-prone compared with stable plaque. **A**, **D**, and **G**, Van Gieson elastin staining (dark purple indicates elastin fibers) shows the presence of organized elastin fibers in the media of control tissue and a net accumulation of elastin fibers in the intima of stable and rupture-prone plaque. **B**–**C**, **E**–**F**, and **H**–**I**, Corresponding immunohistochemistry for tropoelastin (brown staining) shows lack of tropoelastin-positive fibers in control aortas, upregulation in stable, and deposition of a dense network of tropoelastin fibers in rupture-prone plaque. **J**–**K**, Quantification of total elastin and tropoelastin shows significantly higher tropoelastin in ruptured compared with stable plaque. IHC indicates immunohistochemistry.

44.35%±4.83%; *P*=0.03) that includes both the cross-linked and non cross-linked elastin fibers. Only negligible amounts of tropoelastin (7.3%±1.45%) were found in control vessel wall segments compared with elastin (26.3%±0.9%).

Ex Vivo Molecular MRI of Tropoelastin in Human Carotid Endarterectomy Samples

To test the translational value of the tropoelastin contrast agent, we performed ex vivo T_1 mapping experiments after soaking the tissues in Gd-TESMA. The MRI results showed retention of Gd-TESMA and significant increase in the R_1 relaxation rate of carotid plaques ($R_{1\ pre}$=[1.1±0.26]/s versus $R_{1\ post}$=[3.0±0.1]/s; *P*=0.01; Figure 8A–8E), and the histological analyses showed upregulation of tropoelastin in the lesion (Figure 8F–8H).

DISCUSSION

Elastolysis and ineffective elastogenesis favor the accumulation of tropoelastin, rather than mature cross-linked elastin fibers, in atherosclerosis and may trigger plaque progression and instability (6). We have identified tropoelastin-binding peptides and developed a novel gadolinium-based tropoelastin-binding contrast agent that can be used for MRI of tropoelastin turnover in atherosclerosis. We demonstrate that the newly developed Gd-TESMA probe (Gd-DOTA)-VVGS (1) has high selectivity for tropoelastin, (2) discriminates between tropoelastin and cross-linked elastin, (3) has high in vitro relaxivity (r_1) that increases on binding to tropoelastin in solution, and (4) has favorable pharmacokinetics with blood clearance within 1 hour via renal excretion. Using (Gd-DOTA)-VVGS, we demonstrate, for the first time, the feasibility of in vivo imaging of tropoelastin turnover in a murine model of atherosclerotic plaque progression and response to treatment and in a rabbit model of plaque instability. In addition, we show the potential for this novel contrast agent to bind to symptomatic plaques taken from patients undergoing carotid endarterectomy. Molecular imaging of tropoelastin in mice showed increased vessel wall enhancement and R_1 relaxation rates during plaque progression compared with statin-treated and control animals. Histology and Western blotting confirmed the accumulation of tropoelastin within the growing lesion, and inductively coupled plasma mass spectrometry confirmed the accumulation of gadolinium in the vessel wall. Molecular imaging of tropoelastin in rabbits showed significantly higher R_1 relaxation rates in rupture-prone compared with stable lesions showing potential for the detection of high-risk plaques with high sensitivity and specificity. Finally, molecular imaging of human carotid endarterectomy specimens showed detection of intraplaque tropoelastin after soaking the tissues in Gd-TESMA, suggesting that this contrast agent has potential in man. Noninvasive quantification of dysfunctional tropoelas-

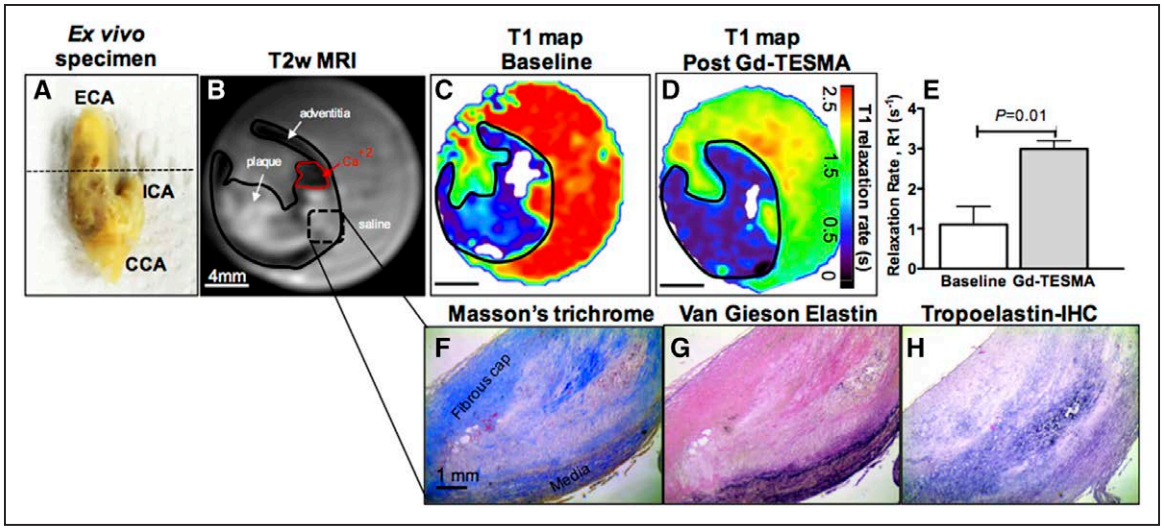

Figure 8. Ex vivo T1 mapping experiments using human carotid endarterectomy specimens at 3T. **A**, Ex vivo photograph of an excised left carotid artery. **B**–**C**, A T2-weighted image shows the plaque in the internal carotid artery (**B**), and a corresponding T1 map shows the baseline relaxation values (**C**). **D**, A repeated T1 mapping experiment after soaking the specimen in Gd-tropoelastin-specific magnetic resonance contrast agent (TESMA) shows a reduction of the T1 values. **E**, Quantification of the changes shows a significant uptake of Gd-TESMA in human carotid plaques. Corresponding histology shows the lesion (**F**–**G**) and the deposition of tropoelastin (dark purple staining; **H**). MRI indicates magnetic resonance imaging. CCA indicates common carotid artery; ECA, external carotid artery; ICA, internal carotid artery; IHC, immunohistochemistry.

tin turnover, that fails to cross-link into mature elastin fibres, using a newly developed tropoelastin-binding MR contrast agent, may therefore have diagnostic value in detecting not only plaque progression and response to treatment but also detection of unstable atherosclerotic lesions before plaque rupture.

The main targeted Gd-based low molecular weight contrast agents that have been developed bind to proteins including fibrin (EP-1873 and EP-2104R),[48] collagen (EP-3533 and EP-3600),[49,50] and elastin (BMS 753951 and LMI 1174)[34,40,46] that are highly abundant and thus amenable for MRI. Most of these agents were initially developed as DTPA chelates and then modified to DOTA chelates to increase their thermodynamic and kinetic stability,[48] and all are clear from blood within 1 to 2 hours after injection. Compared with these agents, our new tropoelastin agent with a single Gd-DOTA conjugated to the N-terminal of the 15 amino acid peptide (2 kDa) showed comparable affinity ($K_D \approx \mu$mol/L), relaxivities, and pharmacokinetics to these agents.[34,35,39,48–50]

Previous studies have shown that the VVGS[11,12,51] probe is expected to bind to all sequences that follow the GXXPG and XGXPG motif (where X is a hydrophobic amino acid) that repeats multiple times in the tropoelastin molecule. In murine tropoelastin, these commonly repeated sequences represent 21% of the entire molecule[52] that may explain our observation of higher vessel wall inductively coupled plasma mass spectrometry gadolinium measurements compared with the tropoelastin concentration as measured by Western blotting. The in vivo vessel wall bound relativity of (Gd-DOTA)-VVGS was 7.15 $(mmol/L)^{-1}$ s^{-1}, and the image acquisition window lasted up to 1.5 hours post-injection. As some of the binding sites of tropoelastin might be masked and the amount of water is lower within the atherosclerotic lesion, this could explain why the in vivo bound relaxivity was lower compared with the relaxivity in solution. Future improvements of the chemical properties of the agent, for example, by chelating more Gd^{3+} per peptide, or conjugating the peptide to a different chelate unit that enables 2 water molecules in the inner coordination sphere of Gd^{3+} could increase the relaxivity of the free, but more importantly of the bound fraction of the agent, and also prolong the imaging acquisition window to allow better detection of vascular tropoelastin and imaging of larger vascular segments.

Our finding that tropoelastin accumulates within the growing lesion and reduces with statin treatment (using immunohistochemistry and Western blotting) in $ApoE^{-/-}$ mice is in agreement with a previous study.[35] Using Western blotting, we found that tropoelastin accumulation is up to 4-fold increased in the murine plaque, compared with control tissue, and reaches a concentration of ≈2 mg/g of tissue. Although statins directly reduce plaque burden through a lipid-lower mechanism, they were also shown to abolish the down-regulation of lysyl oxidase produced by tumor necrosis factor-α and low-density lipoprotein particles through a RhoA/Rho kinase-dependent mechanism.[26] Normalization of lysyl oxidase could promote cross-linking of the newly synthesized tropoelastin leading to an overall reduction of tropoelastin, as seen in our study.

When compared with the Gd-ESMA, the new tropoelastin agent resulted in a smaller area of contrast uptake at the same time points by MRI in atherosclerotic $ApoE^{-/-}$ mice. A previous study also reported a

higher uptake of (^{153}Gd-DTPA)-ESMA compared with (^{64}Cu–DOTA)-VVGS (13.2% versus 7.2% ID/g).[40] As shown in this and other studies,[35–37,39] Gd-ESMA binds equally to cross-linked elastin and tropoelastin. For this reason, enhancement of endogenous cross-linked elastin in nondiseased arteries was also observed in both mice and rabbits. To this end, Gd-ESMA allows measurement of total elastin content and the percentage increase that occurs from the control to the diseased condition by MRI.

In our current study, we found that quantitative assessment of vessel wall contrast uptake using T_1 mapping after administration of Gd-TESMA improved the detection of rupture-prone plaques compared with Gd-ESMA. Rabbit rupture-prone plaques uptake significantly more Gd-TESMA (higher vessel wall R_1) compared with stable plaques whereas the uptake of Gd-ESMA was similar between the 2 groups (similar R_1 values). The elimination of signal from endogenously present cross-linked elastin, and detection of only immature tropoelastin, using the Gd-TESMA, agent allowed a stronger discrimination between rupture-prone and stable rabbit plaques and high prediction of unstable lesions compared with Gd-ESMA. In our previous study using the same rabbit model,[36] we showed that administration of Gd-ESMA allowed measurement of plaque burden that was significantly increased in diseased vessel walls (higher R_1) compared with control vessels and also improved the assessment of positive vascular remodeling that predicted rupture-prone plaques. Finally, to determine whether tropoelastin could be imaged in human tissue, we performed ex vivo T_1 mapping experiments in carotid plaque samples obtained from endarterectomy and soaked in Gd-TESMA. The MRI results showed retention of the agent in carotid plaques, and the histological analyses revealed increased levels of tropoelastin in these plaques. Our findings are in agreement with studies demonstrating that synthetic VSCMs[23,53] and macrophages[6,8] secrete tropoelastin in rabbit atherosclerotic plaque and human carotid atheroma.

In conclusion, this study shows that the accumulation of tropoelastin is associated with plaque progression and instability in atherosclerotic models. In addition, the novel contrast agent is able to demonstrate the presence in tropoelastin in symptomatic plaques taken from patients supporting a potential role for this novel contrast agent in man.

Study Limitations

Our findings on the value of tropoelastin as a marker of plaque burden and instability rely on the use of animal models of atherosclerosis that reflect, only partly, the complex composition of human atherosclerotic plaques and their evolution toward rupture. Although a small intermediate step of using ex vivo human endarterectomy specimens was used to show the translational potential of our work, future studies including larger numbers of human samples will be needed. In addition, the ability of molecular imaging of tropoelastin to detect rupture-prone plaques was based on a relatively small a number of rabbits, and larger animal studies will be need to confirm these findings.

A potential limitation of our study is that an independent BB (eg, double inversion recovery) sequence for the entire vessel wall anatomy was not acquired for the murine experiments. Instead, we implemented a flow-independent delayed-enhancement MRI protocol that was clinically established for myocardial infarction and coronary vessel wall imaging in humans instead of a flow-dependent BB MRI. Another limitation our study was the lack of an automated/semiautomated software for region-of-interest analysis, which was performed manually for all experiments. Future implementation of threshold-based segmentation algorithms may improve vessel wall segmentation and reduce observer bias. Despite the initial potential of using the tropoelastin agent for imaging human plaques, further optimization and extensive safety checks will be needed before using this agent for in vivo imaging of tropoelastin in man.

Conclusions

We demonstrate the development of a new tropoelastin-binding contrast agent and the first in vivo implementation of molecular imaging of tropoelastin in animal models of plaque progression and instability and show uptake of the agent human carotid plaques ex vivo. Tropoelastin may represent a new imaging biomarker for plaque progression and instability and for the monitoring of the effectiveness of therapeutic interventions.

ARTICLE INFORMATION

Received November 3, 2017; accepted June 19, 2018.

The Data Supplement is available at https://www.ahajournals.org/doi/suppl/10.1161/CIRCIMAGING.117.007303.

Correspondence

Alkystis Phinikaridou, PhD, King's College London, School of Biomedical Engineering Imaging Sciences, 4th Floor, Lambeth Wing, St Thomas' Hospital, London SE1 7EH, United Kingdom. E-mail alkystis.1.phinikaridou@kcl.ac.uk

Affiliations

School of Biomedical Engineering and Imaging Sciences (A.P., S.L., B.L., M.E.A., R.M.B.), BHF Centre of Excellence, Cardiovascular Division (A.P., S.L., B.L., R.M.B.), Academic Department of Vascular Surgery, Cardiovascular Division (A.S., P.S.), and Wellcome Trust and EPSRC Medical Engineering Center (R.M.B.), King's College London, United Kingdom. Radiology Department, School of Medicine, Pontificia Universidad Católica de Chile, Santiago (M.E.A.). Pontificia Universidad Católica de Chile, Escuela de Ingeniería, Santiago, Chile (R.M.B).

Acknowledgments

We acknowledge Drs Maria Thanou and Michael Wright (Institute of Pharmaceutical Science, KCL) for their input on the in vitro binding assays. We thank Dr Éva Tóth (Centre de Biophysique Moléculaire, CNRS, Orléans, France) for access to the relaxometer, advice, and analysis of those measurements. We also thank David Onthank Lantheus Medical Imaging (North Billerica) who provided the Gd-elastin-specific magnetic resonance contrast agent for the experiments.

Sources of Funding

This study was funded by the British Heart Foundation (BHF; RG/12/1/29262), the BHF Centre of Excellence (RE/08/03), the Chilean Agency of Technology and Science (CONICYT - PIA - Anillo ACT1416) and by the EU's H2020 research and innovation program under the grant agreement No. 633937 (SPCCT). This work was also supported by the Wellcome EPSRC Centre for Medical Engineering at King's College London (WT 203148/Z/16/Z) and the Department of Health through the National Institute for Health Research comprehensive Biomedical Research Centre award to Guy's & St Thomas' National Health Service (NHS) Foundation Trust in partnership with King's College London and King's College Hospital NHS Foundation Trust.

Disclosures

None.

REFERENCES

1. Sidney S, Rosamond WD, Howard VJ, Luepker RV; National Forum for Heart Disease and Stroke Prevention. The "heart disease and stroke statistics–2013 update" and the need for a national cardiovascular surveillance system. *Circulation*. 2013;127:21–23. doi: 10.1161/CIRCULATIONAHA.112.155911
2. Cannon B. Cardiovascular disease: biochemistry to behaviour. *Nature*. 2013;493:S2–S3. doi: 10.1038/493S2a
3. Robert L, Robert AM, Jacotot B. Elastin-elastase-atherosclerosis revisited. *Atherosclerosis*. 1998;140:281–295.
4. Maurice P, Blaise S, Gayral S, Debelle L, Laffargue M, Hornebeck W, Duca L. Elastin fragmentation and atherosclerosis progression: the elastokine concept. *Trends Cardiovasc Med*. 2013;23:211–221. doi: 10.1016/j.tcm.2012.12.004
5. Brooke BS, Bayes-Genis A, Li DY. New insights into elastin and vascular disease. *Trends Cardiovasc Med*. 2003;13:176–181.
6. Krettek A, Sukhova GK, Libby P. Elastogenesis in human arterial disease: a role for macrophages in disordered elastin synthesis. *Arterioscler Thromb Vasc Biol*. 2003;23:582–587. doi: 10.1161/01.ATV.0000064372.78561.A5
7. Haust MD, More RH, Bencosme SA, Balis JU. Elastogenesis in human aorta: an electron microscopic study. *Exp Mol Pathol*. 1965;4:508–524.
8. Xu C, Zarins CK, Pannaraj PS, Bassiouny HS, Glagov S. Hypercholesterolemia superimposed by experimental hypertension induces differential distribution of collagen and elastin. *Arterioscler Thromb Vasc Biol*. 2000;20:2566–2572.
9. Heinz A, Jung MC, Jahreis G, Rusciani A, Duca L, Debelle L, Weiss AS, Neubert RH, Schmelzer CE. The action of neutrophil serine proteases on elastin and its precursor. *Biochimie*. 2012;94:192–202. doi: 10.1016/j.biochi.2011.10.006
10. Wise SG, Weiss AS. Tropoelastin. *Int J Biochem Cell Biol*. 2009;41:494–497. doi: 10.1016/j.biocel.2008.03.017
11. Hinek A, Rabinovitch M. 67-kD elastin-binding protein is a protective "companion" of extracellular insoluble elastin and intracellular tropoelastin. *J Cell Biol*. 1994;126:563–574.
12. Moroy G, Ostuni A, Pepe A, Tamburro AM, Alix AJ, Héry-Huynh S. A proposed interaction mechanism between elastin-derived peptides and the elastin/laminin receptor-binding domain. *Proteins*. 2009;76:461–476. doi: 10.1002/prot.22361
13. Finnis ML, Gibson MA. Microfibril-associated glycoprotein-1 (MAGP-1) binds to the pepsin-resistant domain of the alpha3(VI) chain of type VI collagen. *J Biol Chem*. 1997;272:22817–22823.
14. Brown-Augsburger P, Broekelmann T, Mecham L, Mercer R, Gibson MA, Cleary EG, Abrams WR, Rosenbloom J, Mecham RP. Microfibril-associated glycoprotein binds to the carboxyl-terminal domain of tropoelastin and is a substrate for transglutaminase. *J Biol Chem*. 1994;269:28443–28449.
15. Fischer GM, Swain ML, Cherian K. Increased vascular collagen and elastin synthesis in experimental atherosclerosis in the rabbit. Variation in synthesis among major vessels. *Atherosclerosis*. 1980;35:11–20.
16. Katsuda S, Kaji T. Atherosclerosis and extracellular matrix. *J Atheroscler Thromb*. 2003;10:267–274.
17. Gandhi RH, Irizarry E, Cantor JO, Keller S, Nackman GB, Halpern VJ, Newman KM, Tilson MD. Analysis of elastin cross-linking and the connective tissue matrix of abdominal aortic aneurysms. *Surgery*. 1994;115:617–620.
18. Curran ME, Atkinson DL, Ewart AK, Morris CA, Leppert MF, Keating MT. The elastin gene is disrupted by a translocation associated with supravalvular aortic stenosis. *Cell*. 1993;73:159–168.
19. Nili N, Zhang M, Strauss BH, Bendeck MP. Biochemical analysis of collagen and elastin synthesis in the balloon injured rat carotid artery. *Cardiovasc Pathol*. 2002;11:272–276.
20. Brasselet C, Durand E, Addad F, Al Haj Zen A, Smeets MB, Laurent-Maquin D, Bouthors S, Bellon G, de Kleijn D, Godeau G, Garnotel R, Gogly B, Lafont A. Collagen and elastin cross-linking: a mechanism of constrictive remodeling after arterial injury. *Am J Physiol Heart Circ Physiol*. 2005;289:H2228–H2233. doi: 10.1152/ajpheart.00410.2005
21. Robinson PN, Arteaga-Solis E, Baldock C, Collod-Béroud G, Booms P, De Paepe A, Dietz HC, Guo G, Handford PA, Judge DP, Kielty CM, Loeys B, Milewicz DM, Ney A, Ramirez F, Reinhardt DP, Tiedemann K, Whiteman P, Godfrey M. The molecular genetics of Marfan syndrome and related disorders. *J Med Genet*. 2006;43:769–787. doi: 10.1136/jmg.2005.039669
22. Nikkari ST, Järveläinen HT, Wight TN, Ferguson M, Clowes AW. Smooth muscle cell expression of extracellular matrix genes after arterial injury. *Am J Pathol*. 1994;144:1348–1356.
23. Belknap JK, Grieshaber NA, Schwartz PE, Orton EC, Reidy MA, Majack RA. Tropoelastin gene expression in individual vascular smooth muscle cells. Relationship to DNA synthesis during vascular development and after arterial injury. *Circ Res*. 1996;78:388–394.
24. Rodríguez C, Alcudia JF, Martínez-González J, Guadall A, Raposo B, Sánchez-Gómez S, Badimon L. Statins normalize vascular lysyl oxidase down-regulation induced by proatherogenic risk factors. *Cardiovasc Res*. 2009;83:595–603. doi: 10.1093/cvr/cvp136
25. Rodríguez C, Alcudia JF, Martínez-González J, Raposo B, Navarro MA, Badimon L. Lysyl oxidase (LOX) down-regulation by TNFalpha: a new mechanism underlying TNFalpha-induced endothelial dysfunction. *Atherosclerosis*. 2008;196:558–564. doi: 10.1016/j.atherosclerosis.2007.06.002
26. Rodríguez C, Martínez-González J, Raposo B, Alcudia JF, Guadall A, Badimon L. Regulation of lysyl oxidase in vascular cells: lysyl oxidase as a new player in cardiovascular diseases. *Cardiovasc Res*. 2008;79:7–13. doi: 10.1093/cvr/cvn102
27. Rodríguez C, Raposo B, Martínez-González J, Casaní L, Badimon L. Low density lipoproteins downregulate lysyl oxidase in vascular endothelial cells and the arterial wall. *Arterioscler Thromb Vasc Biol*. 2002;22:1409–1414
28. Huffman MD, Curci JA, Moore G, Kerns DB, Starcher BC, Thompson RW. Functional importance of connective tissue repair during the development of experimental abdominal aortic aneurysms. *Surgery*. 2000;128:429–438. doi: 10.1067/msy.2000.107379
29. Mäki JM, Räsänen J, Tikkanen H, Sormunen R, Mäkikallio K, Kivirikko KI, Soininen R. Inactivation of the lysyl oxidase gene Lox leads to aortic aneurysms, cardiovascular dysfunction, and perinatal death in mice. *Circulation*. 2002;106:2503–2509.
30. Li DY, Brooke B, Davis EC, Mecham RP, Sorensen LK, Boak BB, Eichwald E, Keating MT. Elastin is an essential determinant of arterial morphogenesis. *Nature*. 1998;393:276–280. doi: 10.1038/30522
31. Van Herck JL, De Meyer GR, Martinet W, Van Hove CE, Foubert K, Theunis MH, Apers S, Bult H, Vrints CJ, Herman AG. Impaired fibrillin-1 function promotes features of plaque instability in apolipoprotein E-deficient mice. *Circulation*. 2009;120:2478–2487. doi: 10.1161/CIRCULATIONAHA.109.872663
32. Van der Donckt C, Van Herck JL, Schrijvers DM, Vanhoutte G, Verhoye M, Blockx I, Van Der Linden A, Bauters D, Lijnen HR, Sluimer JC, Roth L, Van Hove CE, Fransen P, Knaapen MW, Hervent AS, De Keulenaer GW, Bult H, Martinet W, Herman AG, De Meyer GR. Elastin fragmentation in atherosclerotic mice leads to intraplaque neovascularization, plaque rupture, myocardial infarction, stroke, and sudden death. *Eur Heart J*. 2015;36:1049–1058. doi: 10.1093/eurheartj/ehu041
33. Senior RM, Griffin GL, Mecham RP. Chemotactic activity of elastin-derived peptides. *J Clin Invest*. 1980;66:859–862. doi: 10.1172/JCI109926
34. Onthank D, Yalamanchili P, Cesati R, Lazewatsky J, Azure M, Hayes M, Kavosi M, Spencer K, Sousa D, Wexler E, Lamoy M, Harris T, Hu C, Jones R, Dwyer G, Casebier D, Robinson S. Abstract 1914: BMS753951: a novel low molecular weight magnetic resonance contrast agent selective for arterial wall imaging. *Circulation*. 2007;116:II 411–II 412.

35. Makowski MR, Wiethoff AJ, Blume U, Cuello F, Warley A, Jansen CH, Nagel E, Razavi R, Onthank DC, Cesati RR, Marber MS, Schaeffter T, Smith A, Robinson SP, Botnar RM. Assessment of atherosclerotic plaque burden with an elastin-specific magnetic resonance contrast agent. *Nat Med*. 2011;17:383–388. doi: 10.1038/nm.2310
36. Phinikaridou A, Andia ME, Indermuehle A, Onthank DC, Cesati RR, Smith A, Robinson SP, Saha P, Botnar RM. Vascular remodeling and plaque vulnerability in a rabbit model of atherosclerosis: comparison of delayed-enhancement MR imaging with an elastin-specific contrast agent and unenhanced black-blood MR imaging. *Radiology*. 2014;271:390–399. doi: 10.1148/radiol.13130502
37. Makowski MR, Preissel A, von Bary C, Warley A, Schachoff S, Keithan A, Cesati RR, Onthank DC, Schwaiger M, Robinson SP, Botnar RM. Three-dimensional imaging of the aortic vessel wall using an elastin-specific magnetic resonance contrast agent. *Invest Radiol*. 2012;47:438–444. doi: 10.1097/RLI.0b013e3182588263
38. Botnar RM, Wiethoff AJ, Ebersberger U, Lacerda S, Blume U, Warley A, Jansen CH, Onthank DC, Cesati RR, Razavi R, Marber MS, Hamm B, Schaeffter T, Robinson SP, Makowski MR. *In vivo* assessment of aortic aneurysm wall integrity using elastin-specific molecular magnetic resonance imaging. *Circ Cardiovasc Imaging*. 2014;7:679–689. doi: 10.1161/CIRCIMAGING.113.001131
39. von Bary C, Makowski M, Preissel A, Keithahn A, Warley A, Spuentrup E, Buecker A, Lazewatsky J, Cesati R, Onthank D, Schickl N, Schachoff S, Hausleiter J, Schömig A, Schwaiger M, Robinson S, Botnar R. MRI of coronary wall remodeling in a swine model of coronary injury using an elastin-binding contrast agent. *Circ Cardiovasc Imaging*. 2011;4:147–155. doi: 10.1161/CIRCIMAGING.109.895607
40. Wildgruber M, Bielicki I, Aichler M, Kosanke K, Feuchtinger A, Settles M, Onthank DC, Cesati RR, Robinson SP, Huber AM, Rummeny EJ, Walch AK, Botnar RM. Assessment of myocardial infarction and postinfarction scar remodeling with an elastin-specific magnetic resonance agent. *Circ Cardiovasc Imaging*. 2014;7:321–329. doi: 10.1161/CIRCIMAGING.113.001270
41. Protti A, Lavin B, Dong X, Lorrio S, Robinson S, Onthank D, Shah AM, Botnar RM. Assessment of myocardial remodeling using an elastin/tropoelastin specific agent with high field magnetic resonance imaging (MRI). *J Am Heart Assoc*. 2015;4:e001851. doi: 10.1161/JAHA.115.001851
42. Chen W, Cormode DP, Vengrenyuk Y, Herranz B, Feig JE, Klink A, Mulder WJ, Fisher EA, Fayad ZA. Collagen-specific peptide conjugated HDL nanoparticles as MRI contrast agent to evaluate compositional changes in atherosclerotic plaque regression. *JACC Cardiovasc Imaging*. 2013;6:373–384. doi: 10.1016/j.jcmg.2012.06.016
43. Christov A, Korol RM, Dai E, Liu L, Guan H, Bernards MA, Cavers PB, Susko D, Lucas A. *In vivo* optical analysis of quantitative changes in collagen and elastin during arterial remodeling. *Photochem Photobiol*. 2005;81:457–466. doi: 10.1562/2004-03-10-RA-107
44. Phinikaridou A, Hallock KJ, Qiao Y, Hamilton JA. A robust rabbit model of human atherosclerosis and atherothrombosis. *J Lipid Res*. 2009;50:787–797. doi: 10.1194/jlr.M800460-JLR200
45. Phinikaridou A, Ruberg FL, Hallock KJ, Qiao Y, Hua N, Viereck J, Hamilton JA. *In vivo* detection of vulnerable atherosclerotic plaque by MRI in a rabbit model. *Circ Cardiovasc Imaging*. 2010;3:323–332. doi: 10.1161/CIRCIMAGING.109.918524
46. Caravan P, Ellison JJ, McMurry TJ, Lauffer RB. Gadolinium(III) chelates as MRI contrast agents: structure, dynamics, and applications. *Chem Rev*. 1999;99:2293–2352.
47. Phinikaridou A, Hua N, Pham T, Hamilton JA. Regions of low endothelial shear stress colocalize with positive vascular remodeling and atherosclerotic plaque disruption: an *in vivo* magnetic resonance imaging study. *Circ Cardiovasc Imaging*. 2013;6:302–310. doi: 10.1161/CIRCIMAGING.112.000176
48. Overoye-Chan K, Koerner S, Looby RJ, Kolodziej AF, Zech SG, Deng Q, Chasse JM, McMurry TJ, Caravan P. EP-2104R: a fibrin-specific gadolinium-Based MRI contrast agent for detection of thrombus. *J Am Chem Soc*. 2008;130:6025–6039. doi: 10.1021/ja800834y
49. Caravan P, Das B, Dumas S, Epstein FH, Helm PA, Jacques V, Koerner S, Kolodziej A, Shen L, Sun WC, Zhang Z. Collagen-targeted MRI contrast agent for molecular imaging of fibrosis. *Angew Chem Int Ed Engl*. 2007;46:8171–8173. doi: 10.1002/anie.200700700
50. Spuentrup E, Ruhl KM, Botnar RM, Wiethoff AJ, Buhl A, Jacques V, Greenfield MT, Krombach GA, Günther RW, Vangel MG, Caravan P. Molecular magnetic resonance imaging of myocardial perfusion with EP-3600, a collagen-specific contrast agent: initial feasibility study in a swine model. *Circulation*. 2009;119:1768–1775. doi: 10.1161/CIRCULATIONAHA.108.826388
51. Hinek A, Rabinovitch M, Keeley F, Okamura-Oho Y, Callahan J. The 67-kD elastin/laminin-binding protein is related to an enzymatically inactive, alternatively spliced form of beta-galactosidase. *J Clin Invest*. 1993;91:1198–1205. doi: 10.1172/JCI116280
52. Houghton AM, Quintero PA, Perkins DL, Kobayashi DK, Kelley DG, Marconcini LA, Mecham RP, Senior RM, Shapiro SD. Elastin fragments drive disease progression in a murine model of emphysema. *J Clin Invest*. 2006;116:753–759. doi: 10.1172/JCI25617
53. Badesch DB, Lee PD, Parks WC, Stenmark KR. Insulin-like growth factor I stimulates elastin synthesis by bovine pulmonary arterial smooth muscle cells. *Biochem Biophys Res Commun*. 1989;160:382–387